An information-theoretic study of fish swimming in the wake of a pitching airfoil

Abstract

Swimming in schools affords several advantages for fish, including enhanced ability to escape from predators, searching for food, and finding correct migratory routes. However, the role of hydrodynamics in coordinated swimming is still not fully understood due to a lack of data-driven approaches to disentangle causes from effects. In an effort to elucidate the mechanisms underlying fish schooling, we propose an empirical study that integrates information theory and experimental biology. We studied the interactions between an actively pitching airfoil and a fish swimming in a flow. The pitching frequency of the airfoil was varied randomly over time, eliciting an information-rich interaction between the airfoil and the fish. Within an information-theoretic framework, we examined the information content of fish tail beating and information transfer from the airfoil to the fish. The proposed framework may help improve our understanding of the role of hydrodynamics in fish swimming, thereby supporting hypothesis-driven studies on the hydrodynamic advantages of fish schooling.

Keywords: Fish schooling, Hydrodynamics, Information theory, Time series, Transfer entropy

1. Introduction

For its geometric complexity and visual allure, fish schooling has attracted the interest of the scientific community and general public for centuries. From herring to tuna, schooling is prevalent across several fish species in salt and fresh waters [1, 2]. The emergence of schooling has often been attributed to the energetic advantages of coordinated swimming [3, 4, 5]. As suggested by Weihs [3] in his seminal work in the 1970s, schooling behavior could be associated with fish preference to form a diamond pattern, where fish in a following position could benefit from the leading fish through vortex-induced pressure variations. More specifically, followers should experience a reduction in the relative flow speed created by the wake of the leaders, thereby reducing the cost of swimming. Past endeavors have offered evidence of the hydrodynamic advantage in schooling fish [4, 5, 6, 7, 8].

The possibility of fish exploiting vortices in the flow has been extensively studied experimentally and numerically. For example, a rainbow trout was found to actively interact with the von Kármán street behind a cylinder by amplifying its body undulations [9]. A decrease in the muscle activity has been observed in fish exploiting vortices, suggesting a reduction in the cost of swimming [10]. Two-dimensional simulations have also confirmed the higher hydrodynamic efficiency of a diamond school pattern compared with solitary swimming fish [11].

However, new studies challenge the complete endorsement of Weihs' explanation, or, at the least, point at some overlooked physical phenomena that warrant further research. For example, three-dimensional numerical simulations of fish swimming at realistic Reynolds numbers ($\mathrm{Re} \sim 10^5$) show that the wake of a fish is not as structured as proposed by Weihs. In addition, simulations do not indicate the presence of vortices near the head of the following fish [5], potentially ruling out the premise that a follower can locate a low-speed flow region and opt to swim therein. Particularly baffling are the recent findings by Ashraf *et al.*[12], which demonstrated that at sufficiently large swimming speeds, fish could leave the diamond pattern in favor of a "phalanx", where there is no leader and all fish beat their tails almost in synchrony. Perhaps, interaction in a phalanx is realized through a faster pathway than vortex-induced pressure, involving surface and pressure waves. This might explain the nearly synchronized motion of the fish and the large

cohesion in the phalanx, although questioning the premise that fish schooling is controlled by vortex-based interactions.

Due to the lack of data-driven techniques to disentangle causes from effects in coordinated swimming, a mathematically-principled understanding of fish schooling remains elusive. We argue that information theory could offer a potent framework for examining the extent and time scale of interactions between fish, in a model-free approach. Adapted from thermodynamics, the concept of entropy has been introduced as a measure of the degree of uncertainty in predicting the outcome of a random variable. For example, considering fish swimming, high information is associated with erratic swimming composed of frequent change of directions and speed, while low-information would relate to steady swimming, where the fish body would bend periodically.

Building upon the seminal work of Shannon [13], information theory has been applied across a disparate range of scientific fields to strengthen our capacity to analyze dynamical processes, support theoretical predictions, and undertake complex diagnostics. For example, Ref. [14] has demonstrated the possibility of using entropy to examine the effect of drug exposure on the locomotor activity of rats. Ref. [15] has put forward a powerful array of entropy-related notions to evaluate the predictability of large-scale turbulence and measure information content in ensemble predictions. Ref. [16] has unveiled new pathways of global energy flow in the climate system which suggest that oceanic surface circulation has a critical role on global temperature.

Despite the burgeoning applications of information theory across research fields, little work has explored the possibility of employing information-theoretic approaches to study hydrodynamic interactions among swimming fish. As a first step toward understanding the hydrodynamics of fish swimming, here, we explore the possibility of studying the hydrodynamic interaction between a live fish and a pitching airfoil through information theory. The premise of using information theory to infer hydrodynamic interactions has been demostrated in our previous work on a fluid-structure interaction problem, in which we studied the interactions between two pitching airfoils through a fluid medium, where pitching dynamics of the airfoils were systematically controlled [17]. We demonstrated the feasibility of an information-theoretic approach to infer which airfoil was actively controlled and which was instead passively responding due to hydrodynamic coupling. We also showed that the strength and time scale of the information flow between the airfoils related to the distance between them and to the hydrodynamic pathway that supported the interaction (vortex advection versus acoustic or surface waves).

Here, we lay the foundations for extending this framework to the study of hydrodynamic interactions in fish schools, by presenting a proof-of-concept experiment on the interaction between an active airfoil and a live fish. Specifically, we designed a swim tunnel to house an actively-controlled pitching airfoil and a live fish. The pitching airfoil was positioned upstream of the fish swimming zone to create disturbances in the flow, similar to those elicited by the tail beat of a leading fish. We simultaneously recorded the pitching angle of the airfoil and the tail beat motion of the fish using a high speed camera for four different flow speeds, from zero to two body lengths per second. Upon these measurements, we pursued an information-theoretic analysis of fish swimming.

First, we scored fish entropy, as a measure of the uncertainty associated with fish swimming. Second, we examined mutual information between the present and the past state of a fish to elucidate the degree of predictability of fish motion. To assess whether fish motion could be partially explained by the pitching of the airfoil, we measured mutual information between them. Finally, to delve more into the influence of the airfoil on the fish, we quantified transfer entropy [18], associated with the improvement in the prediction of the present state of the fish swimming from its past due to additional knowledge about the airfoil pitching. Through a systematic parametric analysis on the key settings of the information-theoretic approach, we attempted at illustrating the flexibility of the implementation, the robustness of the results, and some of the potential limitations of the study.

2. Theoretical background

2.1. Entropy and mutual information

In information theory, the uncertainty of a discrete random variable, X, can be measured through the notion of entropy, originally defined by Shannon [13] as

$$H(X) = -\sum_{x\in\Omega^X} \Pr\{X = x\} \log_2 \Pr\{X = x\}, \quad (1)$$

where $\Pr\{\cdot\}$ denotes probability, x is a realization of X, and the set Ω^X is the sample space that contains all possible realizations of X. By construction, entropy is a nonnegative quantity.

The right hand side of (1) is the opposite of the expectation of the logarithm of the probability mass function, such that the joint entropy of two random variables, X and Y, is defined as [19]

$$H(X,Y) = -\sum_{x\in\Omega^X, y\in\Omega^Y} \Pr\{X=x, Y=y\} \times \log_2 \Pr\{X=x, Y=y\}, \quad (2)$$

where y and Ω^Y are a realization of Y and its sample space, respectively.

A measure of information shared between X and Y is offered by mutual information, defined as [20]

$$\begin{aligned} I(X;Y) &= H(X) + H(Y) - H(X,Y) \\ &= \sum_{x\in\Omega^X, y\in\Omega^Y} \Pr\{X=x, Y=y\} \\ &\quad \times \log_2 \frac{\Pr\{X=x, Y=y\}}{\Pr\{X=x\}\Pr\{Y=y\}}. \end{aligned} \quad (3)$$

Mutual information in (3) is always positive and symmetric. $I(X;Y) = 0$ indicates that X and Y are marginally independent. The definition can be extended to three variables, X, Y, and Z, for which a multivariate mutual information reads [21]

$$\begin{aligned} &I(X;Y;Z) = I(X;Z) + I(Y;Z) - I(X,Y;Z) \\ &= \sum_{x\in\Omega^X, y\in\Omega^Y, z\in\Omega^Z} \Pr\{X=x, Y=y, Z=z\} \log_2 \frac{\Pr\{X=x, Y=y\}\Pr\{Y=y, Z=z\}\Pr\{X=x, Z=z\}}{\Pr\{X=x\}\Pr\{Y=y\}\Pr\{Z=z\}\Pr\{X=x, Y=y, Z=z\}}, \end{aligned} \quad (4)$$

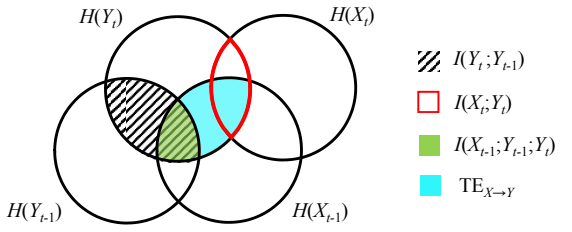

Figure 1: Illustrative Venn diagrams for key information-theoretic quantities.

where z is a realization of Z and Ω^Z is the sample space. $I(X,Y;Z)$ in (4) represents mutual information between Z and (X,Y). Similar to (3), multivariate mutual information defined in (4) is symmetric among X, Y, and Z. However, the value of $I(X;Y;Z)$ can be positive or negative. If we consider Z as a target variable and X and Y as predictor variables, then a positive mutual information can be interpreted as a redundancy in the information provided by X and Y about Z – some information of Z shared by X is also shared by Y. On the other hand, a negative value indicates that X and Y together provide more information about Z than the sum of the information provided individually by X and Y. In other words, there is a synergy in the information of Z provided by X and Y. More information about Z is gained when X and Y are observed together than when they are examined independently.

2.2. *Application to a fish in the wake of a pitching airfoil*

Given an ensemble of stationary discrete stochastic processes, equations (1), (3), and (4) can be used to study information encoded in each process as well as information flow between them. In this article, we describe the dynamics of the airfoil and the fish by focusing on the pitching and tail beat frequency, respectively. Specifically, we use $X = \{X_t\}_{t\in\mathbb{Z}^+}$ and $Y = \{Y_t\}_{t\in\mathbb{Z}^+}$ for the time series of the airfoil pitching frequency and fish tail beat frequency, respectively.

The first information-theoretic measure we examine is the entropy of fish swimming, $H(Y_t)$. Large values of entropy will highlight instances in which the fish randomly changes its tail beat without a preferred beat frequency, while small values of entropy indicates fish swimming at a preferred tail

beat frequency. As shown in Fig. 1, part of the entropy of the fish can be associated with the knowledge of the tail beat frequency at the previous time step (dashed black region). Specifically, we can compute mutual information $I(Y_t; Y_{t-1})$ to measure the amount of information about the current state of the fish, which is encoded in the past state. From (3), this quantity can be expressed as

$$I(Y_t; Y_{t-1}) = H(Y_t) + H(Y_{t-1}) - H(Y_t, Y_{t-1}). \quad (5)$$

This measure encapsulates the degree of predictability of fish swimming from a time step to the next one.

Another portion of the fish entropy could be related to the concurrent pitching of the airfoil, as shown in Fig. 1 (empty red region). Such an instantaneous dependence between the airfoil and the fish is quantified through $I(X_t; Y_t)$ that measures the amount of information about fish swimming that is encoded by the airfoil, namely,

$$I(X_t; Y_t) = H(X_t) + H(Y_t) - H(X_t, Y_t). \quad (6)$$

This quantity can be used as a measure of the interaction between the airfoil and fish at a given time step.

Moving one step forward, we can combine (5) and (6) to form the multivariate mutual information, $I(Y_t; Y_{t-1}; X_{t-1})$, which measures the amount of information in the present state of the fish that is shared with its past and the past state of the airfoil; that is,

$$I(Y_t; Y_{t-1}; X_{t-1}) = I(Y_{t-1}; Y_t) + I(X_{t-1}; Y_t) - I(Y_{t-1}, X_{t-1}; Y_t). \quad (7)$$

The sign of this quantity indicates a redundancy or synergy in the information of Y_t provided by X_{t-1} and Y_{t-1}. A positive value of $I(Y_t; Y_{t-1}; X_{t-1})$ suggests the past states of the fish and the airfoil contain overlapping information about the present state of the fish. A negative value instead indicates that knowing the past state of the fish and the airfoil together conveys more information about the present state of the fish than knowing them independently. Figure 1 also illustrates the notion of multivariate entropy (green region).

Mutual information in (6) quantifies the information shared between the airfoil and the fish. However, testing for independence does not translate into an improved understanding of a potential flow of information from the airfoil to the fish. Such a measurement is critical for the inference of the influence of the airfoil pitching on the fish tail beat frequency. Information flow can be associated with the notion of transfer entropy, coined by Schreiber [18], which reads

$$\begin{aligned} \mathrm{TE}_{X\to Y} =& I(Y_t; X_{t-1}) - I(Y_t; Y_{t-1}; X_{t-1}) \\ =& H(Y_t, Y_{t-1}) - H(Y_{t-1}) \\ & - H(Y_t, Y_{t-1}, X_{t-1}) + H(Y_{t-1}, X_{t-1}). \end{aligned} \quad (8)$$

A graphical representation of transfer entropy is in Fig. 1 (blue region). Transfer entropy is a non-negative quantity that measures the reduction in the uncertainty in the prediction of the future state of Y from its present, due to additional knowledge about the present of X. In alignment with Wiener's principle of causality [22], such a reduction can be attributed to a directional interaction between X and Y. If the airfoil does not influence the fish, then $I(Y_t; X_{t-1}) = I(Y_t; Y_{t-1}; X_{t-1})$, and the value of $\mathrm{TE}_{X\to Y}$ is zero. On the other hand, if the airfoil influences the fish, $\mathrm{TE}_{X\to Y}$ would be positive, indicating that the past state of the airfoil contains additional information for the prediction of the current state of the fish.

Estimation of the probability mass functions poses a major challenge to the accuracy of the entropy computation [20]. Here, we adopted a symbolic representation of the data, which has been used in economics, medical science, and genetics [23, 24, 25], as well as in the study of animal locomotion [14, 26, 27, 28]. Specifically, we used binary symbols such that for a time series $\{x_t\}_{t=1}^{N}$ of length N, $x_t \leq x_{t+1}$ is associated with the symbol 1 and $x_t > x_{t+1}$ is associated with -1. A symbolic representation has a three-fold advantage: i) reducing the effect of measurement noise [29]; ii) mitigating the problem of selecting a threshold for binning [30]; and iii) affording robust estimation of information-theoretic quantities from sparse datasets [31].

The proposed symbolic representation reduces the computation of entropies to the estimation of at most $2^3 = 8$ values for the probability of all the possible triplets in (7) and (8). These probability values were then computed using plug-in estimators based on the experimental time series [32].

3. Experimental design

3.1. Setup

Experiments were carried out in a water tunnel (Engineering Laboratory Design, Inc.) with a $240 \times 15 \times 15\,\mathrm{cm}^3$ (length×height×width) test section. A smaller swimming area within the test section was constructed by placing two honeycomb flow straighteners $L = 30\,\mathrm{cm}$ apart, as shown in Fig. 2. Metal meshes were used as side walls in the swimming area to mitigate boundary layer growth, which may cause potential confounds due to unwanted regions of low fluid velocity. The top of the test section was sealed with an acrylic board to maintain a height of approximately 10 cm, to help in mitigating the effect of surface waves; also, the panel created a high contrast white background for image tracking from below the test section.

The experiments were recorded using a Nikon D7000 camera at 30 frames per second with a resolution of 1280×720 pixels, corresponding to a field of view of $37 \times 21\,\mathrm{cm}^2$ (length×width). A fluorescent light was used to illuminate the test section from the top of the water tunnel. A 3D-printed NACA 0012 airfoil with a chord length of 5 cm (corresponding approximately to the fish body length) and a span of 8 cm was situated in the center of the water tunnel at the upstream margin of the swimming area. Actuation was realized through an external servomotor connected to a metal rod. The motion of the servomotor was controlled by an Arduino Uno microcontroller (Arduino Uno, Arduino, Italy), which was programmed using the MATLAB support package for Arduino.

Prior to experimental trials, extensive particle image velocimetry (PIV) [33] was undertaken to characterize the flow field throughout the test section. The PIV system consisted of a Raypower continuous-wave laser with 532 nm wavelength, a Phantom high-speed camera, and a timer box (Dantec Dynamics, Skovlunde, Denmark). Polyamid particles of 50 μm in diameter were used as seeding particles. In the absence of the airfoil and the fish, PIV results showed uniform velocity profiles for all flow rates tested between 5.0 cm/s and 10.0 cm/s. Flow fields in the wake of the pitching airfoil were also visualized through PIV. Under each flow rate, particle motion was recorded for 10 airfoil pitching cycles at a constant pitching frequency f. Particle images were then used to quantify the velocity field around the airfoil.

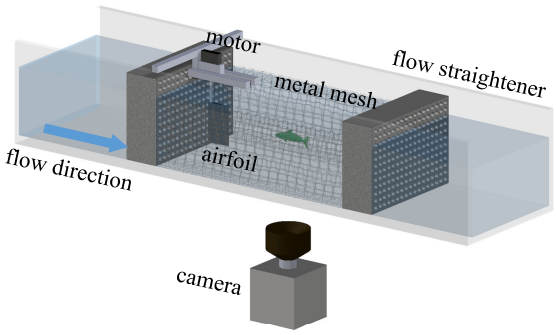

Figure 2: Schematic of the fish swim tunnel setup.

Figure 3: Photograph of a giant danio. The white bar is 2 cm in length.

3.2. Animals

Experiments were performed in accordance with relevant guidelines and regulations approved by the University Animal Welfare Committee (UAWC) of New York University under protocol number 13-1424.

In our study, 60 adult giant danios (*Devario aequipinnatus*) were used for testing, each with a body length between 5 and 7 cm (Fig. 3). Giant danio is a highly social species [34], which in their natural environment live in fast moving streams and channels [35]. Fish were purchased from an online vendor (LiveAquaria.com, Rhinelande, WI, USA) in May 2018 and were housed in a 615-liter vivarium. Water was kept at a temperature of $25 \pm 1°\mathrm{C}$ and a pH of 7.2. Fish were exposed to a 12-h light and 12-h dark period and were fed with flake food between 6:00 and 7:00 pm every day.

3.3. Experimental procedure

Four different flow speeds (U), $U_0 = 0\,\mathrm{cm/s}$, $U_1 = 5.0\,\mathrm{cm/s}$, $U_2 = 7.5\,\mathrm{cm/s}$, and $U_3 = 10.0\,\mathrm{cm/s}$, corresponding to approximately 0, 1.0, 1.5, and 2.0 body lengths per second, respectively, were tested. These flow speeds span a typical range of swimming speeds of groups of schooling giant danios observed in laboratory settings [36].

Table 1: Airfoil pitching frequencies for each flow speed.

U (cm/s)	0	5.0	7.5	10.0
$\overline{\text{TBF}} - 3\Delta\text{TBF}$ (Hz)	2.25	2.25	2.75	3.25
$\overline{\text{TBF}}$ (Hz)	3.00	3.00	3.50	4.00
$\overline{\text{TBF}} + 3\Delta\text{TBF}$ (Hz)	3.75	3.75	4.25	4.75

Table 2: Estimated time scale of flow advection expressed as multiples of airfoil pitching cycles for all pitching frequencies and nonzero flow speeds.

U (cm/s)	5.0	7.5	10.0
$\overline{\text{TBF}} - 3\Delta\text{TBF}$	11.25	9.17	8.13
$\overline{\text{TBF}}$	15.00	11.67	10.00
$\overline{\text{TBF}} + 3\Delta\text{TBF}$	18.75	14.16	11.88

At the beginning of each trial, the water speed in the tunnel was set to zero, and a single fish was hand-netted from the vivarium and introduced into the water tunnel for an initial 5-minute habituation session to the new environment. Then, the flow speed was changed to the desired value and maintained for a second habituation period of 2.5 minutes, followed by another 2.5 minutes of habituation during which the airfoil was commanded to pitch between $\pm 5^\circ$. A final testing phase of 5 minutes was recorded under the same condition using a high speed camera. A total of 15 fish were tested at each flow speed. At the end of each trial, the fish was released back to a separated section of the vivarium.

During each trial (last 2.5-minute habituation session and 5-minute testing phase), the airfoil was actuated at a constant pitching frequency for 10 cycles, before switching to a potentially different value, uniformly drawn from the set $\{\overline{\text{TBF}} - 3\Delta\text{TBF}, \overline{\text{TBF}}, \overline{\text{TBF}} + 3\Delta\text{TBF}\}$ (Table 1), where $\overline{\text{TBF}}$ and ΔTBF are the mean and standard deviation of the tail beat frequency of the fish swimming at the corresponding flow speed in the absence of the airfoil as determined from pilot tests. For each flow speed, in Table 1 we present the three possible values of the pitching frequency of the airfoil.

The rationale for this actuation scheme is to create an information-rich dynamic interaction with hydrodynamically-salient changes, while allowing the fish sufficient time to adjust to the incoming flow generated by the airfoil. The choice of the time duration of 10 pitching cycles for each frequency is based on the advection time scale, T, of the flow structures generated by the airfoil. For nonzero flow speeds, the advection time scale can be estimated from the distance from the trailing edge of the airfoil to the end of the swim tunnel ($D \approx 25$ cm) as $T = D/U$. Hence, the time scale at which the fish should respond to the flow disturbances from the airfoil should vary between 8 and 19 airfoil pitching cycles for non-zero flow speeds, as shown in Table 2. Therefore, maintaining 10 consecutive cycles for each pitching frequency should be sufficient for the flow disturbances associated with a specific pitching frequency to be perceived by the fish in almost the entire test section. At the same time, changing the pitching frequencies every 10 cycles allowed for implementing about one hundred pitching frequencies in the 5-min testing phase.

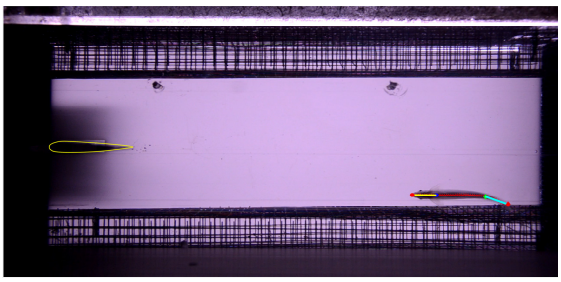

Figure 4: Underneath camera view of the swim tunnel during an experimental test, showing a fish swimming downstream of the airfoil. The center line of the fish body is indicated by a red line. The fish heading and tail beat orientation are indicated by yellow and green lines, respectively. The airfoil is shown in yellow.

3.4. Data analysis

The pitching frequency of the airfoil and the tail beat frequency of the fish were estimated from the video images using a custom-built MATLAB program (Fig. 4). Each of the time series contains 9000 data points obtained at 30 frames per second. Briefly, to track the fish tail beating, each frame of the video was extracted and binarized based on a predetermined threshold, such that the dark fish body would be converted to black and the light background to white. The centerline of the fish was identified as the locus of the centroids of each vertical slice of black pixels, see the red line in Fig. 4. The heading and the tail orientation were identified by fitting two straight lines on the front and back quarters of the fish centerline. The tail beat angle of the fish was defined as the angle between the

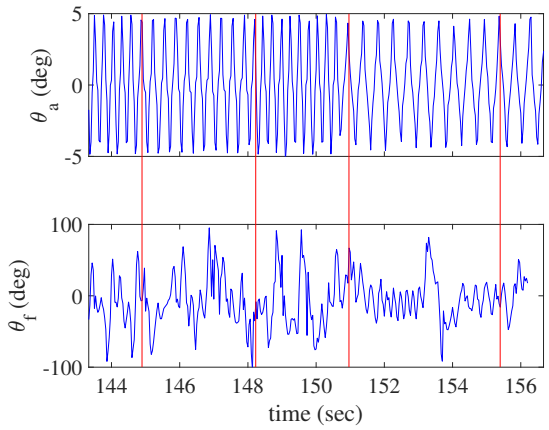

Figure 5: An exemplary segment of the tracked airfoil pitching angle θ_a (top) and the fish tail beat angle θ_f (bottom). θ_a is binned every 10 beating cycles, with the bin locations indicated by red lines. θ_f is binned using the same bin locations.

heading and tail orientation. Tracking of the airfoil followed an equivalent process, but a different threshold was used to facilitate the identification of the trailing edge from the background. The pitching angle of the airfoil was then computed from the trailing edge position.

Exemplary segments of the airfoil pitching angle, θ_a, and the fish tail beat angle, θ_f, are shown in Fig. 5. The two time series of the airfoil pitching and fish tail beat angles were then converted into pitching and tail beat frequencies. First, the local maxima of θ_a were identified from Fig. 5, to label the beginning of a pitching cycle. Then, the pitching angles were aggregated for $w = 10$ consecutive cycles, starting from the time of the switching of the airfoil pitching frequency, t_{sw}, indicated by the red vertical lines in Fig. 5. Coarser and finer resolutions were also explored in our analysis, with w attaining values smaller or larger than 10.

The analysis of the time series of the tail beat angle of the fish was synchronized with the switching of airfoil pitching angle frequencies. Within each window, we computed the total number of tail beats by counting the number of local maxima in θ_f (Fig. 5~~(b)~~). An average tail beat frequency was obtained by dividing the number of tail beats by the time span of the window. Exemplary time series of the airfoil pitching and fish tail beat frequencies are shown in Fig. 6. Each time series contained $N = 80$ to 120 data points, depending on the pitching frequencies of the airfoil, as indicated in Table 1.

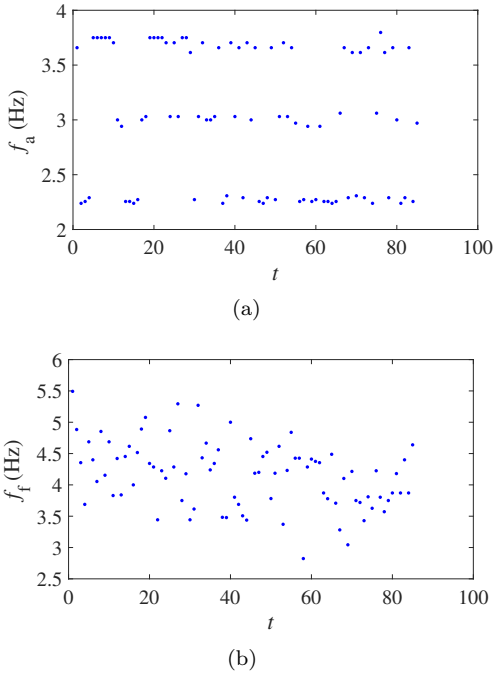

Figure 6: Time series of (a) the airfoil pitching frequency and (b) fish tail beat frequency derived from the time series of the angles partially shown in Fig. 5.

Frequency data were ultimately summarized into binary symbols based on the relative increase and decrease of consecutive data points, which was used as input for our information-theoretic analysis, entailing the study of the entropy of fish swimming (1), the predictability of fish swimming from the past to the current state (5), the instantaneous dependence of fish swimming on the airfoil pitching (6), and information flow from the airfoil to the fish (8).

Utilizing binary symbols, the total number of possible combinations of all the triplets in Eq. (7) and (8) is $2^3 = 8$, resulting in 10 to 15 observations available for each combination. The use of a larger embedding dimensions would lead to some of the combinations not even being observed in the available time series. For example, an embedding dimension of three would lead to a total of $(3!)^3 = 216$ combinations, which is roughly twice the number of available observations.

The use of a window of 10 cycles is consistent with the unitary delay underlying our transfer entropy analysis. As detailed in Table 2, the time scales associated with the advection of vortices from the tip of the pitching airfoil vary from 8 to 19 cycles

for nonzero flow speeds, corresponding to a delay of approximately one time step between the time series of the airfoil pitching frequency and the fish tail beat frequency.

To test the influence of the flow speed on the selected information-theoretic measures, linear regression fits were conducted on the values of entropy $H(Y_t)$, mutual information $I(Y_t; Y_{t-1})$ and $I(X_t; Y_t)$, and transfer entropy $\mathrm{TE}_{X\to Y}$ computed from all 60 trials with the speed as the independent variable. Significance was ascertained with $p = 0.050$.

We used surrogate data sets to test the statistical significance of the values of $I(X_t; Y_t)$ and $\mathrm{TE}_{X\to Y}$. First, under each flow speed, we randomly paired the 15 time series of the airfoil with the 15 time series of fish by shuffling. Each pair was converted into binary symbols for the computation of $I(X_t; Y_t)$ and $\mathrm{TE}_{X\to Y}$. Mean values of $I(X_t; Y_t)$ and $\mathrm{TE}_{X\to Y}$ were obtained from the 15 random pairs and used as surrogate data points in a fictitious experiment in which the fish and the airfoil could not have interacted. This process was repeated 20000 times to generate empirical probability distributions for the mean of $I(X_t; Y_t)$ and $\mathrm{TE}_{X\to Y}$. A significance level of 0.050 was used to test if the measured, mean, values of $I(X_t; Y_t)$ and $\mathrm{TE}_{X\to Y}$ were in the right tail of the corresponding surrogate distribution. Note that this nonparametric statistical test requires no assumption on the distribution of the data [37, 38].

To delve into the hydrodynamics of the interaction between the airfoil and the fish, we visualized the spatial preference of the fish and the wake structure created by the pitching airfoil. Spatial preference was estimated by spatially discretizing the camera view of the swim tunnel with a square mesh of 0.25×0.25 mm^2. The spatial preference of the fish was scored as the probability of the fish residing in an element during each experimental test. For each flow rate, we created a heatmap of the averaged spatial preference from the total of 15 fish.

The instantaneous velocity field around the pitching airfoil was measured by cross-correlating subsequent particle images recorded before the experimental trials on fish, as explained in Sec. 3.1. Cross-correlation was conducted in an open source software, PIVlab [39], built in MATLAB. For each flow speed, a mean velocity field was obtained by averaging instantaneous velocity fields over 10 pitching cycles at the nominal pitching frequency $\overline{\mathrm{TBF}}$ in Table 1. To quantify the turbulence intensity of the flow in the wake of the airfoil from the instantaneous velocity fields, we extracted the variation of the velocity magnitude over time at the center of the swimming section and computed its root-mean-square deviation.

4. Results

4.1. Information-theoretic measures

Entropy of fish swimming, computed on tail beat frequency data, is displayed in Table 3. For all flow speeds, entropy values are close to the maximum theoretical value of one, suggesting that fish did not cruise at a steady tail beat frequency, but considerably varied their tail beat frequency throughout each trial. No dependence of the entropy on the flow speed U was identified from linear regression [1] ($H(Y_t) = 9.61 \times 10^{-5}(U/U_1) + 0.996$; $p = 0.918$).

Table 3 also contains data on mutual information, $I(Y_t; Y_{t-1})$, which is associated with the degree of predictability of fish swimming from its past. For all flow speeds, the value of $I(Y_t; Y_{t-1})$ was on the order of 0.1, suggesting a moderate memory effect on fish swimming, whereby only 10% of the uncertainty on the tail beat frequency could be explained from previous swimming bouts. No dependence of $I(Y_t; Y_{t-1})$ on the flow speed U was found from linear regression ($I(Y_t; Y_{t-1}) = 9.24 \times 10^{-4}(U/U_1) + 0.0893$; $p = 0.917$).

Delving into the potential role of the pitching airfoil in explaining the uncertainty of fish swimming, we computed the mutual information between the current states of the airfoil and the fish tail beat frequencies, $I(X_t; Y_t)$. Mean values and standard deviations are, again, presented in Table 3. Although only 1 to 2% of fish uncertainty is explained by the concurrent pitching of the airfoil, comparison against surrogate data in Fig. 7 indicated that $I(X_t; Y_t)$ was significant at $U = U_1$ ($p = 0.045$). For $U = U_0$, we registered a marginally significant result ($p = 0.050$). Also, we found a dependence of mutual information on the flow speed, whereby linear regression indicated that $I(X_t; Y_t)$ was negatively related to U ($I(X_t; Y_t) = -0.0049(U/U_1) + 0.0175$; $p = 0.033$).

Moving one step forward in the study of the interaction between the airfoil and the fish, we scored

[1] In the fits, the scaling by a characteristic velocity is needed to ensure that all the coefficients are nondimensional.

Table 3: Mean and standard error of information-theoretic measures.

U (cm/s)	0	5.0	7.5	10.0
$H(Y_t)$ (bits)	0.996 ± 0.001	0.997 ± 0.001	0.994 ± 0.002	0.997 ± 0.001
$I(Y_t; Y_{t-1})$ (bits)	0.097 ± 0.013	0.071 ± 0.008	0.099 ± 0.018	0.094 ± 0.009
$I(X_t; Y_t)$ (bits)	0.017 ± 0.003	0.015 ± 0.004	0.008 ± 0.004	0.008 ± 0.003
$\mathrm{TE}_{X\to Y}$ (bits)	0.027 ± 0.008	0.025 ± 0.006	0.013 ± 0.002	0.010 ± 0.002

transfer entropy from the airfoil to the fish swimming. Mean values and standard deviations are, again, collated in Table 3. As one might expect, transfer entropy readings were higher than those of mutual information, reaching approximately 3%. Comparison with surrogate data in Fig. 8 indicated that $\mathrm{TE}_{X\to Y}$ was significant ($p = 0.022$) at $U = U_0$. A trend was seen at $U = U_1$, where we observed that $\mathrm{TE}_{X\to Y}$ fell in the right tail of the distribution but its p-value was larger than significance ($p = 0.137$). As the flow speed increased, the magnitude of $\mathrm{TE}_{X\to Y}$ decreased, as evidenced from linear regression ($\mathrm{TE}_{X\to Y} = -0.0093(U/U_1) + 0.0295$; $p = 0.012$).

4.2. Visualization of the interaction

Interaction between the airfoil and the fish is visualized via the heatmap of the fish spatial preference and the flow velocity field in the wake of the airfoil. The spatial preference heatmap shows that the incoming flow has an effect on fish behavior, whereby the heatmap at $U = U_0$ is qualitatively different from $U = U_1$, U_2, and U_3. At $U = U_0$, fish swam uniformly in the tunnel without a preferred location (Fig. 9(a)), whereas at any other speed, fish exhibited a preference for a downstream location near the outlet of the swim section, as shown in Fig. 9(c)–(g).

Similarly, the flow field in the wake of the airfoil exhibit distinct flow structures in the absence of a background flow. At $U = U_0$, vortices generated by the airfoil diffuse in the vicinity of the airfoil (Fig. 9(b)), while they are advected downstream by the mean flow, if present (Fig. 9(d)–(h)).

4.3. Parametric analysis of information-theoretic measures

To explore the dependence of the information-theoretic measures on the implementation of the framework, we conducted a parametric analysis, in which we examined: i) data resolution, in the form of variations in the window size w for the computation of the pitching and tail beat frequencies; ii) uncertainty, in the form of noisy sampling times for the acquisition window, and iii) potentially delayed interactions, through the use of a non-unitary time delay in the computation of transfer entropy.

Computation of information-theoretic measures can potentially be affected by the resolution of the time series. We systematically varied the size of the discretization windows, w, and evaluated the values of entropy, mutual information, and transfer entropy through (1), (5), (6), and (8). To assess the effect of finer data resolution, we used $w = 2$ and 5; on the other hand, to examine a coarser data resolution, we utilized $w = 20$.

We found that the mean values of $H(Y_t)$ were close to the maximum value of one for all flow speeds, U, and window sizes, w. Mean values of $I(Y_t; Y_{t-1})$ were on the order of 0.1 for all U and w. Through comparison with surrogate data, $I(X_t; Y_t)$ was found to be significantly larger than chance only at the smallest window size $w = 2$ for $U = U_2$. Values of $\mathrm{TE}_{X\to Y}$ were indistinguishable from chance for all values of U and w. Linear regression indicated that $H(Y_t)$ varied with the flow speed U for all resolutions $w = 2$, 5, and 20, while $I(Y_t; Y_{t-1})$ only at $w = 2$ and 5. No dependence on U was found for $I(X_t; Y_t)$ and $\mathrm{TE}_{X\to Y}$; details are presented in Appendix A.

A potential confound in the analysis of the time series is associated with the sampling time of the data [30], which in our study affects the aggregation of the time series in each window for the calculation of the pitching and tail beat frequency. To explore the effect of the sampling time, we introduced uncertainty in the identification of the switching times, t_{sw}, such that the time series were not exactly aggregated every 10 cycles as in Fig. 5. Experimentally, such an uncertainty may arise from the imperfection in the mechanical actuation of the airfoil. Specifically, we added a random noise to the times, t_{sw}, such that the time series of angles

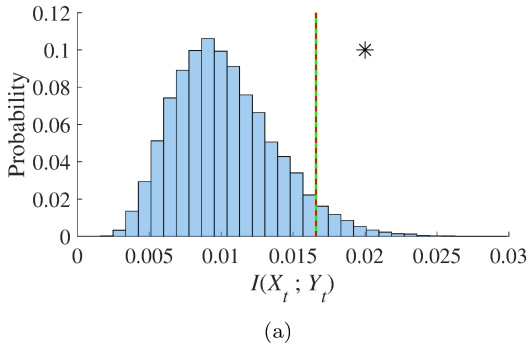

(a)

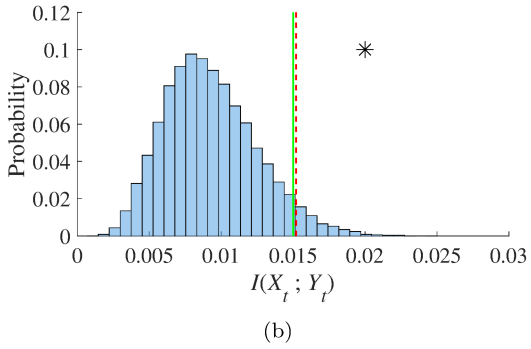

(b)

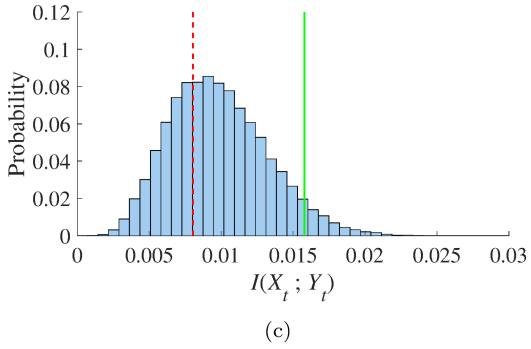

(c)

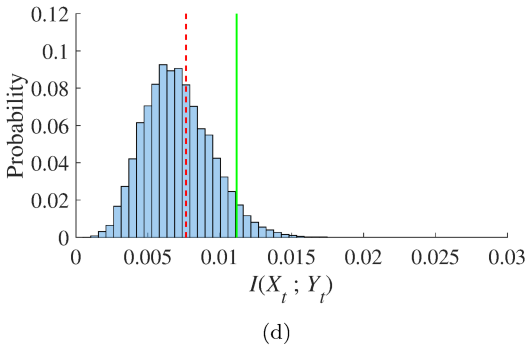

(d)

Figure 7: Mean values of $I(X_t;Y_t)$, in bits, compared with surrogate data set. Probability distribution (bars) are generated from the mean values of $I(X_t;Y_t)$ over 20000 surrogate data points at (a) $U = U_0$, (b) $U = U_1$, (c) $U = U_2$, and (d) $U = U_3$. Green lines indicate the 95% quantile of the probability distributions. Red dashed lines represent mean values of $I(X_t;Y_t)$ from Table 3. An asterisk indicates $p \leq 0.050$.

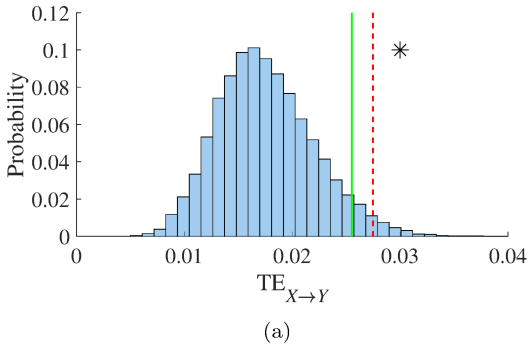

(a)

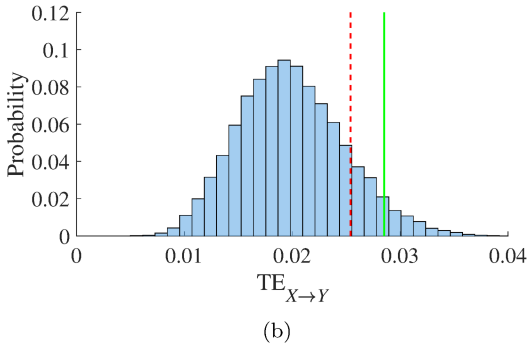

(b)

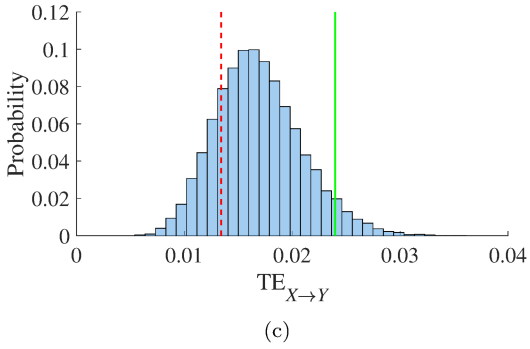

(c)

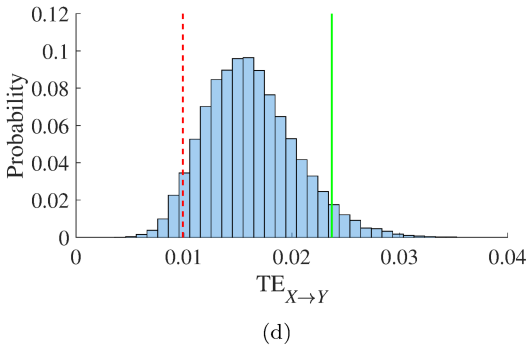

(d)

Figure 8: Mean values of $TE_{X\to Y}$, in bits, compared with surrogate data set. Probability distribution (bars) are generated from the mean values of $TE_{X\to Y}$ over 20000 surrogate data points at (a) $U = U_0$, (b) $U = U_1$, (c) $U = U_2$, and (d) $U = U_3$. Green lines indicate the 95% quantile of the probability distributions. Red dashed lines represent mean values of $TE_{X\to Y}$ from Table 3. An asterisk indicates $p \leq 0.050$.

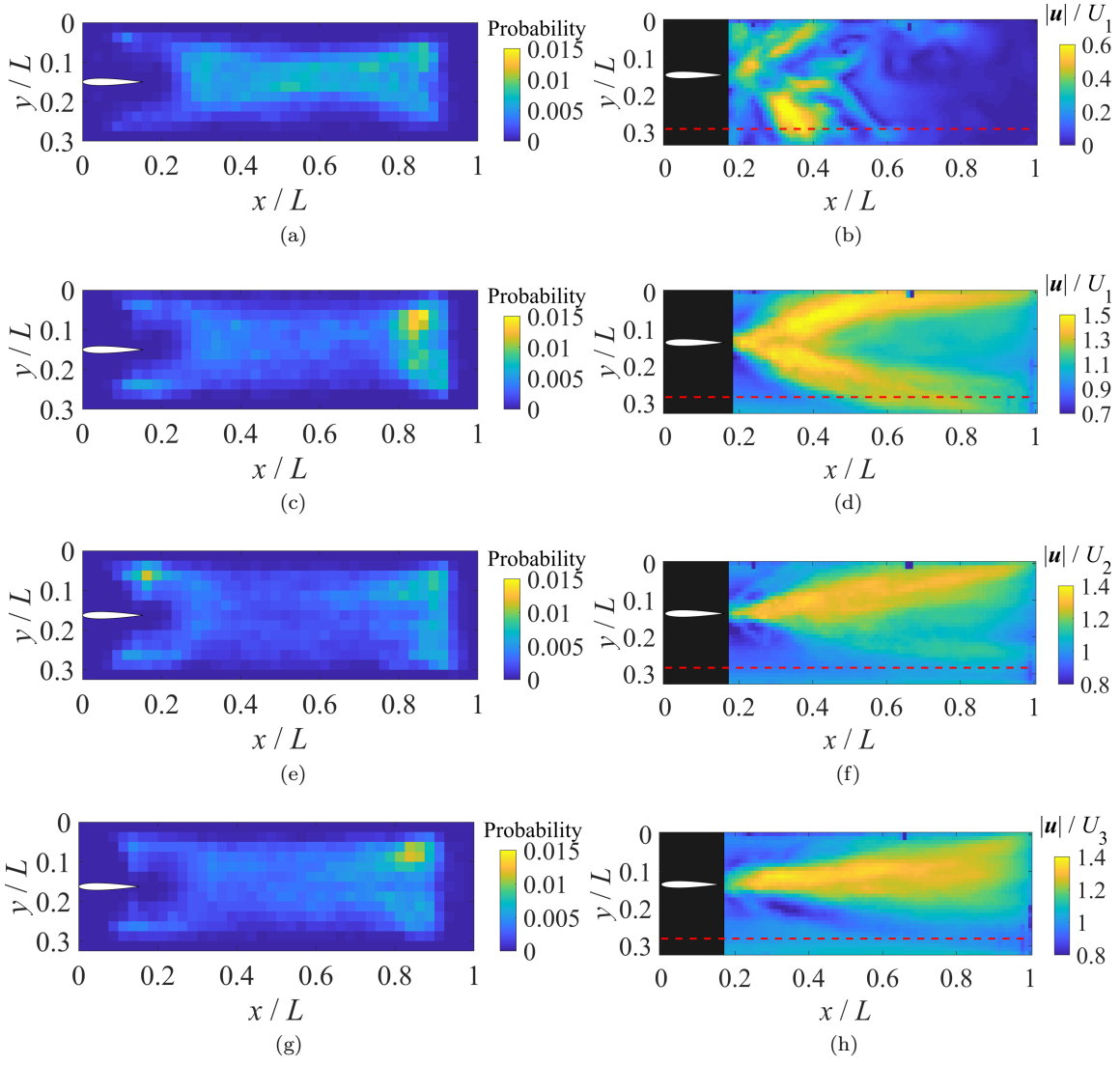

Figure 9: (a, c, e, g) Heatmap of fish spatial preference averaged over 15 individuals at each flow speed. (b, d, f, h) PIV measurements of the flow field in the wake of the pitching airfoil averaged over 10 airfoil beating cycles. Measurements are conducted at (a, b) $U = U_0$, (c, d) $U = U_1$, (e, f) $U = U_2$, and (g, h) $U = U_3$. The root-mean-square deviation of the velocity magnitude over time measured at the center of the swimming section is (b) 0.13 cm/s, (d) 0.94 cm/s, (f) 1.33 cm/s, and (h) 1.44 cm/s, at $U = U_0$, U_1, U_2, and U_3, respectively. The red dashed lines in (b, d, f, h) indicate the mesh location on one side of the tunnel wall, which was removed during PIV measurements to minimize blockage of laser illumination. The airfoil is colored in white.

were partitioned according to new time instants: $t'_{\rm sw} = t_{\rm sw} + \epsilon_n \Delta t$. Here, Δt was the period of a pitching cycle, and ϵ_n was a real number uniformly drawn at random from $[-n, n]$, with $n \in \mathbb{Z}^+$. The values of the entropy, mutual information, and transfer entropy were computed through (1), (5), (6), and (8) for $w = 10$ and $n = 0.1$, 0.2, and 0.5.

We found that the mean values of $H(Y_t)$ were close to the maximum value of one for all flow speeds U and uncertainty levels n. Mean values of $I(Y_t; Y_{t-1})$ were on the order of 0.1 for all n tested. Through comparison with surrogate data, $I(X_t; Y_t)$ was found to be significant only at the lowest uncertainty level $n = 0.1$ for $U = U_0$ and $U = U_1$. Similarly, $\mathrm{TE}_{X\to Y}$ was significant at $n = 0.1$, $U = U_0$ and $n = 0.1$, $U = U_1$. Neither $H(Y_t)$ nor $I(Y_t; Y_{t-1})$ were found to be linearly dependent on the flow speed U for all uncertainty levels n. Linear regression indicated that mutual information $I(X_t; Y_t)$ depended on U for $n = 0.1$ and $n = 0.5$. Transfer entropy $\mathrm{TE}_{X\to Y}$ was found to relate to U only for the lowest uncertainty level $n = 0.1$. Details are presented in Appendix B.

Finally, we examined the effect of time delay on the computation of transfer entropy. The transfer entropy defined in (8) can be generalized to account for interactions at time delays larger than one. To test the influence of the time delay, δ, we computed $\mathrm{TE}_{X\to Y}$ for $\delta = 2$ and 3. Through comparison with surrogate data, we failed to identify statistically significant values of $\mathrm{TE}_{X\to Y}$ for $\delta = 2$ and 3 at all flow speeds U. No dependence of transfer entropy $\mathrm{TE}_{X\to Y}$ on U was found through linear regression for $\delta = 2$ and 3. Details are presented in Appendix C.

5. Discussion and Conclusions

Information theory offers a potent data-driven framework for the study of dynamical processes. Here, we examined the possibility of an information-theoretic approach for the study of a series of controlled experiments, in which a fish swam in the wake of an actively pitching airfoil. To create an information-rich interaction between the airfoil and the fish, pitching frequency of the airfoil was randomly switched over time. Using the time series of the pitching frequency of the airfoil and fish tail beating as inputs, we quantified the uncertainty of fish swimming and examined whether it could be partially or completely explained by previous swimming bouts of the animal or concurrent/past pitching of the airfoil.

The uncertainty of fish swimming was described by Shannon entropy. In agreement with the premise of our experiment to create an information-rich environment for the fish, we recorded high entropy values, $H(Y_t)$, across all flow speeds. About 10% of the information encoded by fish swimming could be explained by previous swimming bouts, as quantified by the mutual information between the present and past state, $I(Y_{t-1}; Y_t)$. Both $H(Y_t)$ and $I(Y_{t-1}; Y_t)$ did not present a dependence on the flow speed, suggesting that the flow speed did not play a significant role on the randomness of fish swimming, which was more likely the outcome of the stochasticity in the dynamics of the airfoil.

The interaction between the airfoil and the fish was studied in terms of mutual information, $I(X_t; Y_t)$, and transfer entropy, $\mathrm{TE}_{X\to Y}$. Mutual information measures the amount of information that is simultaneously (within the same time window of 10 pitching cycles) shared between the fish and the airfoil. However, mutual information does not measure information flow from the airfoil to the fish. In principle, mutual information might reflect shared information between two processes originating from common histories or inputs [40, 41], rather than an authentic dependence between them. Nevertheless, our experiment was unlikely to be conducive to such an experimental confound, given that the pitching airfoil was commanded to randomly switch, independent of the fish. Therefore, the large values of mutual information in the absence of the mean flow and for the lowest flow speed should indicate a stronger dependence of fish swimming on the airfoil pitching.

By controlling for the effect of the past swimming bouts on the present value of the tail beat frequency, transfer entropy offers a more concrete measurement of the potential influence of the airfoil on fish swimming. Only in the absence of a mean flow did we find strong evidence for such an influence, whereby transfer entropy was significantly higher than chance. For the lowest flow speed, we registered a weak trend which does not warrant biologically meaningful conclusions. By varying the time delay in the computation of transfer entropy, we found that this influence had a time scale of approximately 10 pitching cycles, whereby influence was lost when considering 20 or 30 cycles. Both mutual information and transfer entropy suggested that the effect of the airfoil on the fish tended to de-

crease as the flow speed increased, whereby we identified negative dependence of both $I(X_t; Y_t)$ and $\mathrm{TE}_{X\to Y}$ on the flow speed.

Heatmaps of spatial preference and flow field measurements in the wake of the airfoil might help formulate an explanation why the interaction between the airfoil and the fish became negligible at high speeds. Specifically, varying the flow speed changed the time that fish were allotted to react to the incoming coherent structures shed by the airfoil, which, in turn, could be the determining factor of the observed reduction in the interaction. In the absence of the mean flow, $U = U_0$, the coherent structures generated by the airfoil slowly diffused in the otherwise quiescent flow, thereby allowing fish more time to interact with them. This was also evidenced in the spatial heat maps, which suggested that fish swam uniformly in the flow, without a preferential location. The time scale of the interaction with the vortices was on the order of 10 pitching cycles, whereby exploring delayed interactions resulted into values of transfer entropy indistinguishable from chance. On the other hand, at high flow speeds, vortices generated by the airfoil were advected downstream quickly by the mean flow, limiting the time fish can have for reacting. Within this premise, the interaction between the fish and the airfoil detected at the largest flow speed $U = U_2$ using the finest resolution of a window size of two cycles could be a footprint of a potentially faster pathway for interaction, such as visual cues or sound from the motors.

The response of the fish to the airfoil which we detected through information theory in placid flow could be due to fish actively modulating their tail beat to achieve hydrodynamic advantage from the flow. The premise of fish actively exploiting flow structures to obtain hydrodynamic advantages has been observed experimentally [9, 10] through simultaneous measurements of fish swimming pattern, muscle activity, and coherent flow structures. These experiments showed the onset of periodic fish body undulation in response to the passing of vortical structures. Similar evidence was garnered in Ref. [42] through experiments on fish swimming in the wake of a robotic fish, which showed that fish can actively seek to interact with coherent structures to reduce their energy expenditure. Thus, it is tenable that large values of mutual information and transfer entropy could be associated with the fish adjusting their swimming to the varying flow structures from the actively-pitching airfoil.

An alternative explanation for the reduced interaction of the airfoil at higher flow speed may be found in competing needs of efficient swimming and maintaining balance. As the flow speed increased, pitching motion of the airfoil should induce increased turbulence intensity in the flow. The maximum speed at which fish can swim without losing their balance was found to decrease with the turbulence intensity [43, 44, 45]. Maintaining their balance requires a higher level of energy expenditure and may induce higher hydrodynamic drag on the body, due to the use of pectoral fins to achieve body control [44]. At increased flow speed, fish may prioritize the need of maintaining their balance over achieving a favorable hydrodynamic interaction with the wake of the airfoil. This could explain the reduced impact of the airfoil pitching frequency on fish swimming at higher speeds.

Interestingly, at $U = U_1$, we registered a significant interaction between the airfoil and the fish through mutual information, but transfer entropy failed to indicate that this interaction should be interpreted as influence. Perhaps, in the presence of a mean flow, fish could adjust to the flow perturbation produced by the airfoil within a few pitching cycles, thereby reducing the predictive power of the previous state of the airfoil on their current tail beat frequency. Since mutual information was computed on the basis of the same time window of 10 airfoil pitching cycles for the fish and the airfoil, it successfully picked up a dependence between the two processes. However, this explanation is partially challenged by the lack of significant influence at $U = U_1$ when using finer data resolutions, whereby we did not register values of transfer entropy above chance with a window size of 2 or 5 pitching cycles. Future studies could seek to experimentally manipulate the number of cycles at which the airfoil pitched at the same frequency to further elucidate the time scale of a potential influence.

Our predictions were robust with respect to moderate uncertainty in the sampling time, whereby predictions supported by mutual information and transfer entropy were not affected by the added noise. In line with our expectations, increasing the uncertainty in the sampling time caused these predictions to lose statistical significance. Likely, coping with larger levels of uncertainty might be possible by using symbolic embeddings with dimensions larger than two. However, this may call for new experiments, whereby our short time series challenge the use of symbolization richer than the one con-

sidered herein. Interestingly, adding noise did not lead to false positive results, although we recorded a significant value of transfer entropy at intermediate noises and $U = U_1$, where we had only a weak trend in the absence of the added uncertainty. Increasing the number of experiments could help clarify the value of this finding.

Although several other authors have investigated interaction of fish with coherent flow structures, they generally focused on periodic flows. For example, studies of fish swimming in Refs. [9, 10] examined the interaction of fish with a periodic vortex street generated in the wake of a cylinder. Similarly, experiments using robotic fish in Refs. [42, 46] are limited to steady tail beating at a constant frequency by the robot. Our work is different from these studies in that we created an information-rich environment through aperiodic, unsteady flow structures. Either a periodic vortex street behind a cylinder or a steady tail beating by a robotic fish at a constant frequency would lead to a scarcity in information content. The latter would challenge the application of an information-theoretic approach, while failing to faithfully simulate the complexity of fish swimming [47, 48].

Through this methodological study, we demonstrated some of the advantages that are brought about by an information-theoretic approach to fish swimming, while clarifying some of its potential methodological and practical limitations. Information theory may offer a new lens through which we can explore and quantify hydrodynamic interactions without the use of physically-based models. The promising results obtained in our analysis may pave the way for future studies on the hydrodynamic advantages of different fish schooling patterns. One challenge in inferring interactions among multiple individuals using entropy-based measures lies in the accurate estimation of information flow in the presence of possible polyadic dependencies [49]. It is viable that fish swimming in a school may rely on polyadic interactions among one another, in which a fish modulates its behavior according to the locomotion of multiple individuals in the group simultaneously rather than through a pairwise interaction with a particular neighbor. Restraining the analysis to pairwise interactions may fail to unveil the hidden polyadic dependency, thereby leading to an inaccurate representation of interactions within the school. To address this, multivariate conditional entropy may be combined with sophisticated network representation techniques such as hypergraphs [50] and higher order networks [51], which might help unravel polyadic dependencies involving multiple individuals in the fish school.

Acknowledgments

This work was supported by the National Science Foundation under grant numbers CMMI-1505832, CMMI-1433670, and CBET-1332204. The authors thank Maxwell Rosen for his help with pilot tests on fish swimming and Boris Arbuzov for his help with the experiments and video tracking.

Declaration of interest

The authors declare no conflict of interest.

Appendix A. Effect of data resolution on information-theoretic measures

The information-theoretic measures, $H(Y_t)$, $I(Y_t; Y_{t-1})$, $I(X_t; Y_t)$, and $\mathrm{TE}_{X\to Y}$ computed using time series of frequency binned with window sizes $w = 2$, 5, and 20 are detailed in Table A.1.

Mean values of $H(Y_t)$ were close to the maximum value of one for all flow speeds U and window sizes w. Mean values of $I(Y_t; Y_{t-1})$ were on the order of 0.1 for all U and w. Through comparison with surrogate data, $I(X_t; Y_t)$ was found significant only at the smallest window size $w = 2$ for $U = U_2$. No significant value of $\mathrm{TE}_{X\to Y}$ was registered for any U and w.

Linear regression indicated that $H(Y_t)$ depended on the flow speed U for all resolutions $w = 2$, 5, and 20. ($w = 2$: $H(Y_t) = -0.0132(U/U_1) + 0.9983$, $p = 0.006$; $w = 5$: $H(Y_t) = -0.0010(U/U_1) + 0.9990$, $p = 0.017$; $w = 20$: $H(Y_t) = 0.0022(U/U_1) + 0.9932$, $p = 0.027$). $I(Y_t; Y_{t-1})$ was found to be linearly dependent on the flow speed U for $w = 2$ and 5. ($w = 2$: $I(Y_t; Y_{t-1}) = -0.0185(U/U_1) + 0.1028$, $p = 0.052$; $w = 5$: $I(Y_t; Y_{t-1}) = -0.0118(U/U_1) + 0.0822$, $p = 0.025$; $w = 20$: $I(Y_t; Y_{t-1}) = 0.0181(U/U_1) + 0.0872$, $p = 0.877$). No dependence of mutual information $I(X_t; Y_t)$ on U was registered for any w through linear regression ($w = 2$: $I(X_t; Y_t) = 0.0100(U/U_1) + 0.0083$, $p = 0.073$; $w = 5$: $I(X_t; Y_t) = 0.0016(U/U_1) + 0.0052$, $p = 0.094$; $w = 20$: $I(X_t; Y_t) = 0.0030(U/U_1) + 0.0164$,

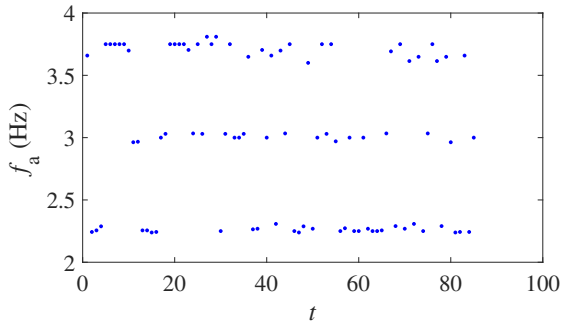

Figure B.1: Time series of airfoil pitching frequency using 10 cycles and an uncertainty level $n = 0.5$.

$p = 0.485$). Similarly, no dependence of transfer entropy $\mathrm{TE}_{X\to Y}$ on U was identified for any w ($w = 2$: $\mathrm{TE}_{X\to Y} = 0.0048(U/U_1) + 0.0210$, $p = 0.378$; $w = 5$: $\mathrm{TE}_{X\to Y} = -0.0007(U/U_1) + 0.0116$, $p = 0.704$; $w = 20$: $\mathrm{TE}_{X\to Y} = -0.0047(U/U_1) + 0.0453$, $p = 0.484$).

Appendix B. Effect of sampling time on information-theoretic measures

Here, we demonstrate the effect of uncertainty in the sampling time on the entropy analysis. An exemplary time series of airfoil pitching frequency derived based on ϵ_n with $n = 0.5$ is displayed in Fig. B.1.

The values of entropy, mutual information, and transfer entropy computed for three levels of noise: $n = 0.1$, 0.2, and 0.5 added to the identification of the switching times t_{sw} for $w = 10$ are displayed in Table B.2. Mean values of $H(Y_t)$ were close to the maximum value of one for all flow speeds U and uncertainty levels n. Mean values of $I(Y_t; Y_{t-1})$ remained on the order of 0.1. Through comparison with surrogate data, $I(X_t; Y_t)$ was found to be significant only at the lowest uncertainty level $n = 0.1$ for $U = U_0$ and $U = U_1$. $\mathrm{TE}_{X\to Y}$ was significant at $n = 0.1$, $U = U_0$ and $n = 0.1$, $U = U_1$.

Neither $H(Y_t)$ or $I(Y_t; Y_{t-1})$ were found to depend on the flow speed U for all uncertainty levels n. Linear regression indicated that mutual information $I(X_t; Y_t)$ depended on U for $n = 0.1$ and $n = 0.5$ ($n = 0.1$: $I(X_t; Y_t) = -0.0069(U/U_1) + 0.0198$, $p = 0.007$; $n = 0.2$: $I(X_t; Y_t) = -0.0044(U/U_1) + 0.0142$, $p = 0.104$; $n = 0.5$: $I(X_t; Y_t) = -0.0052(U/U_1) + 0.0161$, $p = 0.035$). Transfer entropy $\mathrm{TE}_{X\to Y}$ was found to depend on U only for the lowest uncertainty level $n = 0.1$ ($n = 0.1$: $\mathrm{TE}_{X\to Y} = -0.0093(U/U_1) + 0.0302$, $p = 0.013$; $n = 0.2$: $\mathrm{TE}_{X\to Y} = -0.0015(U/U_1) + 0.0211$, $p = 0.663$; $n = 0.5$: $\mathrm{TE}_{X\to Y} = -0.0034(U/U_1) + 0.0189$, $p = 0.189$).

Appendix C. Effect of time delay in transfer entropy analysis

Transfer entropy in (8) can be generalized to account for interactions at time delays larger than one. Based on the definition in [52], at a time delay $\delta \in \mathbb{Z}^+$, transfer entropy from X to Y reads

$$\mathrm{TE}_{X\to Y}(\delta) = \sum_{y_t, y_{t-1}, x_{t-\delta}} \Pr\{Y_t = y_t, Y_{t-1} = y_{t-1}, X_{t-\delta} = x_{t-\delta}\} \times \log_2 \frac{\Pr\{Y_t = y_t | Y_{t-1} = y_{t-1}, X_{t-\delta} = x_{t-\delta}\}}{\Pr\{Y_t = y_t | Y_{t-1} = y_{t-1}\}}. \quad \text{(C.1)}$$

Equation (C.1) quantifies the reduction in the uncertainty in the prediction of the current state of Y from its past, due to additional knowledge of X at δ time steps in the past. The results of $\mathrm{TE}_{X\to Y}$ at delays $\delta = 2$ and 3 are shown in Table C.3.

For $\delta = 2$ and 3, $\mathrm{TE}_{X\to Y}$ was indistinguishable from chance in surrogate data. No dependence of transfer entropy $\mathrm{TE}_{X\to Y}$ on U was found through linear regression for $\delta = 2$ and 3 ($\delta = 2$: $\mathrm{TE}_{X\to Y} = -0.0032(U/U_1) + 0.0174$, $p = 0.118$; $\delta = 3$: $\mathrm{TE}_{X\to Y} = -0.0016(U/U_1) + 0.0168$, $p = 0.514$).

References

[1] T. J. Pitcher, The Behaviour of Teleost Fishes, Croom Helm Ltd, London & Sydney, 1986.

[2] J. Krause, G. D. Ruxton, G. D. Ruxton, Living in Groups, Oxford University Press, 2002.

[3] D. Weihs, Hydromechanics of fish schooling, Nature 241 (5387) (1973) 290–291.

[4] J. Herskin, J. F. Steffensen, Energy savings in sea bass swimming in a school: measurements of tail beat frequency and oxygen consumption at different swimming speeds, Journal of Fish Biology 53 (2) (1998) 366–376.

[5] M. Daghooghi, I. Borazjani, The hydrodynamic advantages of synchronized swimming in a rectangular pattern, Bioinspiration & Biomimetics 10 (5) (2015) 056018.

[6] T. Pitcher, A. Magurran, J. Edwards, Schooling mackerel and herring choose neighbours of similar size, Marine Biology 86 (3) (1985) 319–322.

[7] B. L. Partridge, J. Johansson, J. Kalish, The structure of schools of giant bluefin tuna in cape cod bay, Environmental Biology of Fishes 9 (3) (1983) 253–262.

Table A.1: Mean and standard error of $H(Y_t)$, $I(Y_t;Y_{t-1})$, $I(X_t;Y_t)$, and $\mathrm{TE}_{X\to Y}$ computed based on different aggregation window sizes, w. An asterisk represents a significant result ($p \leq 0.050$) in comparison with surrogate data.

		$U = 0\,\mathrm{cm/s}$	$U = 5.0\,\mathrm{cm/s}$	$U = 7.5\,\mathrm{cm/s}$	$U = 10.0\,\mathrm{cm/s}$
$H(Y_t)$ (bits)	$w = 2$ cycles	0.993 ± 0.002	0.993 ± 0.002	0.984 ± 0.003	0.963 ± 0.013
	$w = 5$ cycles	0.999 ± 0.000	0.998 ± 0.000	0.997 ± 0.001	0.997 ± 0.001
	$w = 20$ cycles	0.994 ± 0.002	0.994 ± 0.002	0.997 ± 0.001	0.998 ± 0.001
$I(Y_t;Y_{t-1})$ (bits)	$w = 2$ cycles	0.113 ± 0.020	0.061 ± 0.007	0.082 ± 0.013	0.072 ± 0.011
	$w = 5$ cycles	0.076 ± 0.006	0.081 ± 0.010	0.069 ± 0.008	0.049 ± 0.005
	$w = 20$ cycles	0.094 ± 0.020	0.079 ± 0.013	0.084 ± 0.015	0.101 ± 0.020
$I(X_t;Y_t)$ (bits)	$w = 2$ cycles	0.013 ± 0.005	0.010 ± 0.003	0.022 ± 0.005*	0.034 ± 0.014
	$w = 5$ cycles	0.005 ± 0.001	0.005 ± 0.002	0.002 ± 0.001	0.002 ± 0.001
	$w = 20$ cycles	0.015 ± 0.005	0.026 ± 0.009	0.015 ± 0.004	0.024 ± 0.006
$\mathrm{TE}_{X\to Y}$ (bits)	$w = 2$ cycles	0.026 ± 0.006	0.018 ± 0.008	0.023 ± 0.006	0.038 ± 0.010
	$w = 5$ cycles	0.010 ± 0.002	0.013 ± 0.003	0.013 ± 0.003	0.008 ± 0.002
	$w = 20$ cycles	0.045 ± 0.011	0.043 ± 0.010	0.035 ± 0.012	0.037 ± 0.006

Table B.2: Mean and standard error of $H(Y_t)$, $I(Y_t;Y_{t-1})$, $I(X_t;Y_t)$, and $\mathrm{TE}_{X\to Y}$ under different levels of uncertainty in the identification of the switching times t_{sw} for $w = 10$ cycles. An asterisk represents a significant result ($p \leq 0.050$) in comparison with surrogate data.

		$U = 0\,\mathrm{cm/s}$	$U = 5.0\,\mathrm{cm/s}$	$U = 7.5\,\mathrm{cm/s}$	$U = 10.0\,\mathrm{cm/s}$
$H(Y_t)$ (bits)	$n = 0.1$	0.996 ± 0.001	0.996 ± 0.001	0.995 ± 0.002	0.997 ± 0.001
	$n = 0.2$	0.996 ± 0.001	0.997 ± 0.001	0.994 ± 0.002	0.999 ± 0.001
	$n = 0.5$	0.996 ± 0.002	0.996 ± 0.001	0.996 ± 0.001	0.999 ± 0.000
$I(Y_t;Y_{t-1})$ (bits)	$n = 0.1$	0.098 ± 0.015	0.077 ± 0.009	0.100 ± 0.019	0.094 ± 0.008
	$n = 0.2$	0.095 ± 0.013	0.078 ± 0.011	0.098 ± 0.015	0.091 ± 0.008
	$n = 0.5$	0.095 ± 0.013	0.070 ± 0.007	0.093 ± 0.015	0.090 ± 0.010
$I(X_t;Y_t)$ (bits)	$n = 0.1$	0.019 ± 0.004*	0.016 ± 0.004*	0.006 ± 0.003	0.007 ± 0.003
	$n = 0.2$	0.013 ± 0.004	0.013 ± 0.007	0.006 ± 0.002	0.005 ± 0.002
	$n = 0.5$	0.014 ± 0.003	0.016 ± 0.006	0.005 ± 0.002	0.006 ± 0.002
$\mathrm{TE}_{X\to Y}$ (bits)	$n = 0.1$	0.028 ± 0.009*	0.024 ± 0.004	0.017 ± 0.003	0.009 ± 0.002
	$n = 0.2$	0.016 ± 0.004	0.030 ± 0.007*	0.016 ± 0.005	0.015 ± 0.004
	$n = 0.5$	0.019 ± 0.005	0.016 ± 0.003	0.014 ± 0.003	0.012 ± 0.003

Table C.3: Mean and standard error of $\mathrm{TE}_{X\to Y}$, in bits, computed at different time delays, δ.

	$U = 0\,\mathrm{cm/s}$	$U = 5.0\,\mathrm{cm/s}$	$U = 7.5\,\mathrm{cm/s}$	$U = 10.0\,\mathrm{cm/s}$
$\delta = 2$	0.018 ± 0.004	0.013 ± 0.003	0.013 ± 0.003	0.012 ± 0.003
$\delta = 3$	0.017 ± 0.004	0.013 ± 0.003	0.018 ± 0.004	0.012 ± 0.003

[8] J. C. Liao, A review of fish swimming mechanics and behaviour in altered flows, Philosophical Transactions of the Royal Society B: Biological Sciences 362 (1487) (2007) 1973–1993.
[9] J. C. Liao, D. N. Beal, G. V. Lauder, M. S. Triantafyllou, The Kármán gait: novel body kinematics of rainbow trout swimming in a vortex street, Journal of Experimental Biology 206 (6) (2003) 1059–1073.
[10] J. C. Liao, D. N. Beal, G. V. Lauder, M. S. Triantafyllou, Fish exploiting vortices decrease muscle activity, Science 302 (5650) (2003) 1566–1569.
[11] C. Hemelrijk, D. Reid, H. Hildenbrandt, J. Padding, The increased efficiency of fish swimming in a school, Fish and Fisheries 16 (3) (2015) 511–521.
[12] I. Ashraf, H. Bradshaw, T.-T. Ha, J. Halloy, R. Godoy-Diana, B. Thiria, Simple phalanx pattern leads to energy saving in cohesive fish schooling, Proceedings of the National Academy of Sciences 114 (36) (2017) 9599–9604.
[13] C. E. Shannon, A mathematical theory of communication, Bell System Technical Journal 27.
[14] M. P. Paulus, M. A. Geyer, L. H. Gold, A. J. Mandell, Application of entropy measures derived from the ergodic theory of dynamical systems to rat locomotor behavior, Proceedings of the National Academy of Sciences 87 (2) (1990) 723–727.
[15] R. Kleeman, A. Majda, Predictability in a model of geophysical turbulence, Journal of the Atmospheric Sciences 62 (8) (2005) 2864–2879.
[16] J. F. Donges, Y. Zou, N. Marwan, J. Kurths, The backbone of the climate network, Europhysics Letters 87 (4) (2009) 48007.
[17] P. Zhang, M. Rosen, S. D. Peterson, M. Porfiri, An information-theoretic approach to study fluidstructure interactions, Journal of Fluid Mechanics 848 (2018) 968986.
[18] T. Schreiber, Measuring information transfer, Physical Review Letters 85 (2) (2000) 461–464.
[19] T. M. Cover, J. A. Thomas, Elements of Information Theory, Wiley, 2006.
[20] T. Bossomaier, L. Barnett, M. Harr, J. T. Lizier, An Introduction to Transfer Entropy: Information Flow in Complex Systems, Springer, 2016.
[21] R. A. A. Ince, Measuring multivariate redundant information with pointwise common change in surprisal, Entropy 19 (7).
[22] N. Wiener, The theory of prediction, Modern Mathematics for Engineers 1 (1956) 125–139.
[23] F. López, M. Matilla-García, J. Mur, M. Ruiz Marín, A non-parametric spatial independence test using symbolic entropy, Regional Science and Urban Economics 40 (2) (2010) 106–115.
[24] M. R. Conaway, Analysis of repeated categorical measurements with conditional likelihood methods, Journal of the American Statistical Association 84 (405) (1989) 53–62.
[25] M. Ruiz-Marín, M. Matilla-García, J. A. G. Cordoba, J. L. Susillo-González, A. Romo-Astorga, A. González-Pérez, A. Ruiz, J. Gayán, An entropy test for single-locus genetic association analysis, BMC Genetics 11 (1) (2010) 19.
[26] P. Faure, H. Neumeister, D. S. Faber, H. Korn, Symbolic analysis of swimming trajectories reveals scale invariance and provides a model for fish locomotion, Fractals 11 (03) (2003) 233–243.
[27] F. G. Schmitt, L. Seuront, J.-S. Hwang, S. Souissi, L.-C. Tseng, Scaling of swimming sequences in copepod behavior: Data analysis and simulation, Physica A: Statistical Mechanics and its Applications 364 (2006) 287 – 296.
[28] M. Porfiri, M. Ruiz Marín, Symbolic dynamics of animal interaction, Journal of Theoretical Biology 435 (2017) 145–156.
[29] C. S. Daw, C. E. A. Finney, E. R. Tracy, A review of symbolic analysis of experimental data, Review of Scientific Instruments 74 (2) (2003) 915–930.
[30] H. Kantz, T. Schreiber, Nonlinear time series analysis, Cambridge university press, 2004.
[31] W. Yao, J. Wang, Differential entropy in nonlinear dynamics complexity analysis, arXiv preprint arXiv:1801.08416.
[32] L. Paninski, Estimation of entropy and mutual information, Neural Computation 15 (6) (2003) 1191–1253.
[33] M. Raffel, C. E. Willert, S. T. Wereley, J. Kompenhans, Particle Image Velocimetry: A Practical Guide, Springer, 2013.
[34] S. V. Viscido, J. K. Parrish, D. Grünbaum, Individual behavior and emergent properties of fish schools: a comparison of observation and theory, Marine Ecology Progress Series 273 (2004) 239–249.
[35] M. M. McClure, P. B. McIntyre, A. R. McCune, Notes on the natural diet and habitat of eight danionin fishes, including the zebrafish danio rerio, Journal of Fish Biology 69 (2) (2006) 553–570.
[36] P. J. Mekdara, M. A. B. Schwalbe, L. L. Coughlin, E. D. Tytell, The effects of lateral line ablation and regeneration in schooling giant danios, Journal of Experimental Biology.
[37] A. P. Holmes, R. C. Blair, J. D. G. Watson, I. Ford, Nonparametric analysis of statistic images from functional mapping experiments, Journal of Cerebral Blood Flow & Metabolism 16 (1) (1996) 7–22.
[38] T. E. Nichols, A. P. Holmes, Nonparametric permutation tests for functional neuroimaging: A primer with examples, Human Brain Mapping 15 (1) (2002) 1–25.
[39] W. Thielicke, E. Stamhuis, PIVlab–towards user-friendly, affordable and accurate digital particle image velocimetry in MATLAB, Journal of Open Research Software 2 (1).
[40] P. L. Williams, R. D. Beer, Generalized measures of information transfer, arXiv preprint arXiv:1102.1507.
[41] R. Kleeman, Information flow in ensemble weather predictions, Journal of the Atmospheric Sciences 64 (3) (2007) 1005–1016.
[42] S. Marras, M. Porfiri, Fish and robots swimming together: attraction towards the robot demands biomimetic locomotion, Journal of The Royal Society Interface 9 (73) (2012) 1856–1868.
[43] E. C. Enders, D. Boisclair, A. G. Roy, The effect of turbulence on the cost of swimming for juvenile atlantic salmon (*Salmo salar*), Canadian Journal of Fisheries and Aquatic Sciences 60 (9) (2003) 1149–1160.
[44] A. I. Lupandin, Effect of flow turbulence on swimming speed of fish, Biology Bulletin 32 (5) (2005) 461–466.
[45] J. C. Liao, A. Cotel, Effects of Turbulence on Fish Swimming in Aquaculture, Springer Berlin Heidelberg, Berlin, Heidelberg, 2013, pp. 109–127.
[46] G. Polverino, P. Phamduy, M. Porfiri, Fish and robots swimming together in a water tunnel: Robot color and tail-beat frequency influence fish behavior, PLoS ONE

8 (10) (2013) 1–10.
[47] J. C. Svendsen, J. Skov, M. Bildsoe, J. F. Steffensen, Intra-school positional preference and reduced tail beat frequency in trailing positions in schooling roach under experimental conditions, Journal of Fish Biology 62 (4) (2003) 834–846.
[48] K. B. Tierney, Swimming performance assessment in fishes, Journal of Visualized Experiments (51).
[49] R. G. James, N. Barnett, J. P. Crutchfield, Information flows? a critique of transfer entropies, Physical Review Letters 116 (2016) 238701.
[50] E. Estrada, J. A. Rodríguez-Velázquez, Subgraph centrality and clustering in complex hyper-networks, Physica A: Statistical Mechanics and its Applications 364 (2006) 581 – 594.
[51] J. Xu, T. L. Wickramarathne, N. V. Chawla, Representing higher-order dependencies in networks, Science Advances 2 (5).
[52] M. Wibral, R. Vicente, J. T. Lizier, Directed Information Measures in Neuroscience, Springer Publishing Company, Incorporated, 2014.